

Rising bubble simulations using a multiple relaxation time lattice Boltzmann method coupled with level set interface capturing

Amin Safi*, Stefan Turek

*Corresponding author; amin.safi@math.tu-dortmund.de

Institute of Applied Mathematics (LSIII), TU Dortmund, Vogelpothsweg 87, D-44221 Dortmund, Germany

Abstract

A multiphase Lattice Boltzmann (LB) scheme coupled with a level set interface capturing module is used for the simulation of multiphase flows, and in particular, rising bubbles under moderate and high density and viscosity ratios. We employ a consistent, robust discretization of the pressure forces along with using multiple relaxation time (MRT) form of the collision in the LB equation which enables us to preserve stability and accuracy. We first present the solution for the standard test of a static bubble in order to show the accuracy of the solution with respect to the Laplace law for pressure and conserving the spurious velocity level. We present quantitative benchmark computations and error analysis for the 2D rising bubble test cases, introduced in [16], which are further compared with the solutions from the so-called Shan-Chen diffused interface LB models as well as with high precision finite element solutions. The accuracy of the present scheme is shown to be competitive with that of the finite element approach, while the nice characteristics of general LB solutions are preserved.

1 Introduction

The use of the lattice Boltzmann method (LBM) has long been a major field of interest for the simulation of multiphase flows [27, 6]. The LBM's mesoscopic nature allows for incorporating the so-called intermolecular forces to the right hand side of the LBE causing the two different phases to reach equilibrium in single or multi-component disciplines [31, 30, 29]. As contrary to the conventional Navier-Stokes approaches, such an implicit interface realization eliminates the need for explicit capturing or tracking of the interface, often assigned to a second equation as in volume of fluid or level set methods [27, 28, 33]. Eventually, diffused interface LB models could generally recover phase change phenomena and do not have to treat topological difficulties in the case of complex bubble or droplet deformations. Such computational characteristics, along with the easy implementation of complex boundary conditions and high scalability for parallel computations has made LBM a favourable candidate for multiphase flow simulations.

Consequently, there has been a number of proposals for schemes to model the relevant intermolecular forces in LBM. Among the most popular diffused interface LB schemes is the Shan-Chen model [31] extensively used in both academic and commercial LBM software packages e. g. PowerFlow [1], OpenLb [2] and Palabos [3]. The model relates the interface force to the intermolecular potential ψ which defines the non-ideal deviation from LBM's ideal gas equation of state (EOS) for the pressure. In fact the EOS controls the phase segregation as it defines the pressure change profile with the change of density based on the Maxwell's equal area rule at certain temperatures [38]. The EOS has also a critical impact on the maximum permissible density ratio between the phases. While the original EOS of the Shan-Chen model in [31] becomes notoriously unstable at density ratios larger than 20, more robust EOS like the R-K or C-S equations allow for density ratios as high

as 1000 in single component two phase problems (e. g. water and its vapour), yet at the price of relatively large spurious velocities around the interface [38].

Nevertheless, in the case of a two component, two phase flow where the viscosities might also be significantly different, even the use of the most sophisticated EOS could not be effective in simulating strictly immiscible mixtures at large density/viscosity differences as the solution has to reach asymptotically zero concentration of the second fluid in the first fluid and vice-versa [4]. Moreover, one has to solve for two sets of LBEs on the entire domain in each time step since each component has its own specific properties.

A major enhancement to the class of diffused interface LB models is proposed by Lee and Lin [20, 18, 19], where they replaced Shan-Chen’s interaction force with the Cahn-Hilliard chemical potential and a pressure evolution LBE is solved for the pressure and momentum instead of density and momentum. Therefore, no EOS has to be adopted to link the pressure and density profiles and the interface is diffusely captured via solving a second LBE for the order parameter (density). Unlike the Shan-Chen model, they were successful in gaining high density and viscosity ratios and low spurious velocities. However, their scheme requires high number of derivatives as needed for the Cahn-Hilliard chemical potential and needs to solve a second LBE (almost as costly as the first one) while the resolution of the interface still depends on that of the underlying mesh for the LBE.

A new trend in the development of multiphase LB models is to confine the LBE to solve for the flow and let a second PDE track the interface. The idea is motivated from the fact that in single bubble or droplet problems, a sharp realization of the instantaneous position of the interface at very high density/viscosity differences and large EO numbers is of paramount importance. Thommes et al. [35] and later Becker et al. [5] followed this strategy for 3D simulations using a two-fluid approach, where each fluid is solved on its own domain, and the interface forces are imposed explicitly by modifying the bounce-back boundary condition on the curved interface such that it includes the surface tension forces. The interface is then captured through solving level set equation. Finally, the method has to go through a re-filling step to re-distribute the two fluid nodes as the boundary between the two fluid changes position in each time step. While their new sophisticated boundary condition is successful in reaching high density differences and capturing sharp interfaces, one has to construct two different mesh spacings on each fluid side in the case of large viscosity ratios, resulting in more mathematical complexity and higher computational costs [35].

As contrary to the two-fluid approach in [35], Mehravaran and Hannani [23, 22] tried to extend the one-fluid approach, widely used in the Navier-Stokes based solutions, towards LBE, i. e. to solve for the momentum using LBE for a single virtual fluid on the entire domain and treat the interface boundary conditions as local smeared-out force terms in the right hand side of the LBE. Similar to [35], they also proposed to capture the interface by solving the level set equation. Nevertheless, their model leaves the calculation of the pressure to a third PDE and hence they do not provide any discussions regarding the accuracy in the pressure field or the spurious velocity level. Furthermore, one could not find validations against the established static or rising bubble solutions and the comparisons are rather restricted to qualitative ones.

In this paper we follow the general idea in the one-fluid approach of Mehravaran and Hannani [22], except that we introduce a consistent discretization of the force and in particular the pressure gradient term. We show that the accurate realization of the pressure jumps across the interface is the key to a reliable solution in case of high density and viscosity differences. As a result, the simple linear EOS of the LB method is demonstrated to remain valid in recovering the correct pressure field even at critical jump conditions. To keep the scheme stable at very low viscosities as well as to minimize the spurious velocities, we employ the multiple relaxation time (MRT) collision scheme. We go through rigorous comparisons and error analysis for the static bubble at different density and viscosity ratios and then evaluate the performance of the model by extensive benchmark comparisons against the finite element solutions for the rising bubble problems as provided using the FeatFLOW package in [16]. The rest of the paper is organized as follows; we present the derivation and discretization of the one-fluid coupled multiphase LB model as well as its multiple relaxation time implementation in section 2. Section 3 elaborates the solution of the level set equation as the interface capturing module. The numerical results and validations for the static and rising bubbles are then provided in section 4. Finally, the paper is closed with conclusions and discussions in section 5.

2 The coupled LB-level set model

2.1 The lattice Boltzmann Equation

The lattice Boltzmann equation describes the evolution of distribution functions in the discretized phase space, i. e. discrete velocity space e. g. in the D2Q9 model in two dimensions, having 9 microscopic velocities e_k , $k = 0, \dots, 8$ [11, 13, 21]. Assuming a single relaxation time (SRT) approximation for the collision of the distribution functions, He and Shan et. al [14] proposed the following LB equation in the presence of the external force F

$$\frac{\partial f_k}{\partial t} + e_k \cdot \nabla f_k = \frac{1}{\tau} (f_k - f_k^{eq}) + \frac{(e_k - \mathbf{u}_i) \cdot F_i}{\rho c_s^2} f_k^{eq} \quad (1)$$

where $c_s = 1/\sqrt{3}$ is the lattice speed of sound and ρ and \mathbf{u} are the macroscopic density and velocity obtained by the zero and first-order moments of distribution functions, respectively

$$\rho = \sum_k f_k \quad , \quad \rho \mathbf{u}_i = \sum_k e_{i,k} f_k \quad (2)$$

and f_k^{eq} is the Maxwell equilibrium ,

$$f_k^{eq} = \omega_k \rho \left[1 + \frac{e_k \cdot \mathbf{u}}{c_s^2} + \frac{(e_k \cdot \mathbf{u})^2}{2c_s^4} + \frac{(\mathbf{u} \cdot \mathbf{u})}{2c_s^2} \right]. \quad (3)$$

Starting from equation (1) and going through the Chapman-Enskog expansion [10] one could recover the Navier-Stokes equations in the nearly incompressible limit:

$$\partial_t(\rho \mathbf{u}) + \partial_i(\rho c_s^2 \delta_{ij} + \rho \mathbf{u}_i \mathbf{u}_j) - \frac{1}{3} \left(\tau - \frac{1}{2} \right) \partial_i [\partial_j(\rho \mathbf{u}_i) + \partial_i(\rho \mathbf{u}_j)] = F_j \quad (4)$$

$$\partial_t(\rho) + \partial_i(\rho \mathbf{u}_i) = 0 \quad (5)$$

A comparison to the standard Navier-Stokes equations reveals that the viscosity is evaluated as $\nu = (\tau - 0.5)/3$ and that the pressure could be recovered as a simple EOS

$$P = \rho c_s^2. \quad (6)$$

For equation (6) to be valid, the flow must remain in the nearly-incompressible regime meaning that the density changes have to be moderate so as to model the pressure gradients within the flow field [32].

2.2 One-fluid multiphase formulation

The one-fluid approach also known as the continuum surface force (CSF) approach for multiphase flow problems consists of solving the Navier-Stokes equations along with the surface tension boundary conditions as local smeared out forces acting on the interface Γ . In that sense, Sussman et al. proposed the following form of the governing equations [34]

$$\rho(\phi)\partial_t\mathbf{u} + \rho(\phi)\mathbf{u} \cdot \nabla\mathbf{u} + \nabla P - \nabla \cdot (\mu(\phi)(\nabla\mathbf{u} + \nabla\mathbf{u}^T)) = -\sigma\kappa(\phi)\delta_\varepsilon(\phi)\mathbf{n}(\phi) \quad (7)$$

$$\nabla \cdot \mathbf{u} = 0 \quad (8)$$

where σ is the surface tension coefficient, δ is the Dirac delta function and κ and \mathbf{n} are the mean curvature and normal vector to the interface, respectively. Equation (7) is then coupled with the level set equation for the advection of the level set function ϕ , initially assumed to be a signed distance function, with fluid velocity \mathbf{u} , while $\phi = 0$ indicates the interface Γ

$$\partial_t\phi + \mathbf{u} \cdot \nabla\phi = 0. \quad (9)$$

As such, the bulk fluid properties could be related to the individual properties of each phase as functions of the signed distance function

$$\begin{cases} \rho(\phi) = \rho_l H(\phi) + \rho_g(1 - H(\phi)) \\ \mu(\phi) = \mu_l H(\phi) + \mu_g(1 - H(\phi)) \end{cases} \quad (10)$$

where $H(\phi)$ is a regularized Heaviside function such as

$$H(\phi) = \begin{cases} 0 & \phi < -\varepsilon \\ \frac{1}{2} \left[1 + \frac{\phi}{\varepsilon} + \frac{1}{\pi} \sin\left(\frac{\pi\phi}{\varepsilon}\right) \right] & |\phi| \leq \varepsilon \\ 1 & \phi > \varepsilon \end{cases} \quad (11)$$

and ε is the interface thickness on each side. Consequently, a smoothed realization of the delta function would be of the form [34]

$$\delta(\phi) = \frac{dH}{d\phi} = \begin{cases} 0 & \phi < -\varepsilon \\ \frac{1}{2} \left[\frac{1}{\varepsilon} + \cos\left(\frac{\pi\phi}{\varepsilon}\right) \right] & |\phi| \leq \varepsilon \\ 0 & \phi > \varepsilon \end{cases} \quad (12)$$

Furthermore, the curvature as well as the normal vector to the interface could be obtained using the level set function ϕ as

$$\mathbf{n}(\phi) = \frac{\nabla\phi}{|\nabla\phi|}, \quad \kappa(\phi) = \nabla \cdot \mathbf{n} = \nabla \cdot \left(\frac{\nabla\phi}{|\nabla\phi|} \right). \quad (13)$$

A direct mapping of the CSF approach, as described above, to the LBM would lead to severe numerical errors since the simple EOS in equation (6) would break down in case of any density changes across the interface and thus may produce non-physical pressure values. Moreover, in the viscous force term in 7 one still has to apply the divergence to the variable viscosity $\mu(\phi)$, and this does not comply with the LBM-derived form in equation (4). In order to remove such unfavourable features, we rewrite the momentum equation (7) in a suitable form for the LBM. Going along the lines of [22], we divide equation (7) by $\rho(\phi)$

$$\partial_t\mathbf{u} + \mathbf{u} \cdot \nabla\mathbf{u} + \frac{\nabla P}{\rho(\phi)} - \frac{\nabla \cdot (\mu(\phi)(\nabla\mathbf{u} + \nabla\mathbf{u}^T))}{\rho(\phi)} = -\frac{\sigma\kappa(\phi)\mathbf{n}(\phi)\delta_\varepsilon(\phi)}{\rho(\phi)}. \quad (14)$$

By introducing a virtual density $\bar{\rho} = 1$ to the convective terms, adding ∇P terms to the both sides and expanding the viscous term as

$$\frac{\nabla \cdot (\mu(\phi)(\nabla \mathbf{u} + \nabla \mathbf{u}^T))}{\rho(\phi)} = -\frac{\mu(\phi)\nabla \cdot (\nabla \mathbf{u} + \nabla \mathbf{u}^T)}{\rho(\phi)} - \frac{\nabla \mu(\phi) \cdot (\nabla \mathbf{u} + \nabla \mathbf{u}^T)}{\rho(\phi)} \quad (15)$$

we end up with a new form of the momentum equation

$$\bar{\rho}(\phi)\partial_t \mathbf{u} + \bar{\rho}(\phi)\mathbf{u} \cdot \nabla \mathbf{u} + \nabla P - \bar{\mu}(\phi)\nabla \cdot (\nabla \mathbf{u} + \nabla \mathbf{u}^T) = \bar{F} \quad (16)$$

where $\bar{\mu} = \mu(\phi)/\rho(\phi)$ is the virtual viscosity. The modified force term \bar{F} is obtained as

$$\bar{F} = -\frac{\sigma\kappa(\phi)\mathbf{n}(\phi)\delta_\varepsilon(\phi)}{\rho(\phi)} + \frac{\nabla \mu(\phi) \cdot (\nabla \mathbf{u} + \nabla \mathbf{u}^T)}{\rho(\phi)} + \nabla P \left(1 - \frac{1}{\rho(\phi)}\right). \quad (17)$$

Using equations (10) and (12) we have $\nabla \mu(\phi) = (\mu_l - \mu_g)\delta_\varepsilon(\phi)\nabla \phi$ and hence

$$\bar{F} = -\frac{\sigma\kappa(\phi)\mathbf{n}(\phi)\delta_\varepsilon(\phi)}{\rho(\phi)} + \frac{(\mu_l - \mu_g)\delta_\varepsilon(\phi)}{\rho(\phi)} [\nabla \phi \cdot (\nabla \mathbf{u} + \nabla \mathbf{u}^T)] + \nabla P \left(1 - \frac{1}{\rho(\phi)}\right). \quad (18)$$

The above reformulation means that the virtual density $\bar{\rho}$ is decoupled from the variable physical density. As this virtual density is assumed to be only nearly incompressible, the LBM's EOS is expected to be valid to obtain the pressure as $P = \bar{\rho}c_s^2$. One could also see that \bar{F} comes with two new terms; the first one accounts for the jump in the viscose force term, while the second one adds the effect of the pressure jump across the interface through the ∇P term.

2.3 LBE discretization

2.3.1 Time integration

The new form of the momentum equation (16) along with $\bar{\rho}$ and $\bar{\mu}$ is now suitable to be casted into an LBE-like equation (1) which carries a new force term \bar{F} on the right hand side. Starting from equation (1), we use a forward Euler time integration for the collision term along with the CrankNicolson scheme for the force term to have [24]

$$f_k(x + e_k \Delta t, t + \Delta t) - f_k(x, t) = -\sum_j \Lambda_{k,j}(f_j(x, t) - f_j^{eq}(x, t)) + \frac{\Delta t}{2} S_k \Big|_{(x,t)} + \frac{\Delta t}{2} S_k \Big|_{(x+e_k \Delta t, t+\Delta t)} \quad (19)$$

where Λ is the generalized relaxation matrix and S_k is defined as

$$S_k = \frac{(e_{k,i} - \mathbf{u}_i) \cdot \bar{F}_i}{\bar{\rho}c_s^2} f_k^{eq}. \quad (20)$$

To render the LBE into an explicit form we use the transformation $g_k = f_k - \frac{\Delta t}{2} S_k$ suggested by Premnath and Abraham [26]

$$g_k = f_k - \frac{\Delta t}{2} S_k \quad (21)$$

$$g_k^{eq} = f_k^{eq} - \frac{\Delta t}{2} S_k \quad (22)$$

to obtain

$$g_k(x + e_k \Delta t, t + \Delta t) = g_k(x, t) - \sum_j A_{k,j} (g_j(x, t) - g_j^{eq}(x, t)) + (I - \frac{1}{2} A_{k,j}) S_j(x, t). \quad (23)$$

In the practical implementation, the above equation is carried out in two steps, namely the on-site *collision* step

$$g_k^*(x, t) = g_k(x, t) - \sum_j A_{k,j} (g_j(x, t) - g_j^{eq}(x, t)) + (I - \frac{1}{2} A_{k,j}) S_j(x, t) \quad (24)$$

followed by *streaming* to the neighbouring nodes

$$g_k(x + e_k \Delta t, t + \Delta t) = g_k^*(x, t) \quad (25)$$

As a result of the transformation, we recover the fluid pressure and velocity using the zero- and first-order moments of the new distribution function g_k , respectively,

$$\bar{\rho} \mathbf{u}_i = \sum_k e_{k,i} g_k + 0.5 \bar{F}_i, \quad P = c_s^2 \bar{\rho} = c_s^2 \sum_k g_k. \quad (26)$$

2.3.2 Force discretization

Considering equation (18) for the force \bar{F} , we need to discretize the derivatives ∇P for the pressure force term, $\nabla \mathbf{u}$ as in the viscous force term, and $\nabla \phi$ for calculating $\mathbf{n}(\phi)$ and $\kappa(\phi) = \nabla \cdot \mathbf{n}$ in the surface tension force, respectively (see equation (13)). The most straightforward, second order accurate approach to obtain the first derivatives (∇a in general) would be to use the central differencing scheme along the main X and Y directions

$$\begin{aligned} \nabla_x a(x, y) &= \frac{a(x+h, y) - a(x-h, y)}{2h} \\ \nabla_y a(x, y) &= \frac{a(x, y+h) - a(x, y-h)}{2h} \end{aligned} \quad (27)$$

where h is the mesh spacing. This simple differencing, however, may result in low degree of isotropy, and therefore less accuracy particularly in the pressure field if applied to ∇P . In fact, a closer look at S_k in equation (20) reveals that the term $e_k \cdot \bar{F}$ comprises the directional derivatives of pressure; $e_k \cdot \nabla P$. Moreover, due to the EOS, we have that $O(e_k \cdot \nabla P) \approx O(e_k \cdot \nabla f_k)$, and hence the term $e_k \cdot \nabla P$ contributes to the convection term in the left hand side of the LBE. These observations bring us to the following conclusions

- The contribution to the convective term justifies the semi-implicit Crank-Nicolson time integration
- The differencing for $e_k \cdot \nabla P$ has to be carried out along the lattice directions instead of the main directions
- As the pressure jumps across the interface, one has to pick a discretization mechanism for $e_k \cdot \nabla P$ which is robust enough to capture the sharp jumps and is at least second order accurate

While using a second order upwind differencing leads to fluctuations in the pressure field, a simple central differencing imposes strong dissipation error and hence could not capture the rather sharp pressure jumps across the interface. Consequently, we choose the following averaged scheme which combines the effect of a second order upwinding (w.r.t the $-e_k$ direction) with the central differencing

$$(e_k \cdot \nabla P)^{avg} = \frac{(e_k \cdot \nabla P)^C + (e_k \cdot \nabla P)^U}{2} \quad (28)$$

where the directional central and upwind derivations are calculated as:

$$\begin{aligned} (e_k \cdot \nabla P)^C &= \frac{P(x+e_k \Delta t) - P(x-e_k \Delta t)}{2} \\ (e_k \cdot \nabla P)^U &= \frac{-P(x+2e_k \Delta t) + 4P(x+e_k \Delta t) - 3P(x)}{2}. \end{aligned} \quad (29)$$

It will be further shown in section 4 that such an averaged directional approach for $e_k \cdot \nabla P$ results in significant improvement over the simple central differencing for recovering the correct pressure field and w.r.t. lower spurious velocities in case of high density ratios. A similar effect is reported in the chemical potential model of Lee and Lin [20] for the gradients of the macroscopic density, where they prove through extensive numerical experiments for 1D model problems, that the averaged differencing delivers the optimal numerical efficiency.

To find non-directional derivatives of the pressure ∇P , as required for example in the calculation of $\mathbf{u} \cdot \nabla P$ in S_k (see equation (20)) we make use of the following weighted summation over the central directional derivatives of the pressure [20]

$$\partial_i P = \sum_k w_k \frac{e_{k,i} \cdot (e_k \cdot \nabla P)^C}{c_s^2 \Delta t}. \quad (30)$$

We summarise that using the above discretization scheme in two dimension, one needs to compute a total of 6 central derivatives for $\nabla \phi$, $\nabla \cdot \mathbf{n}$ and $\nabla \mathbf{u}$, plus 8 directional derivatives for $e_k \cdot \nabla P$. On the other hand, one may only require 8 central differences in case of using the naive central derivatives for all the gradients.

2.4 Multiple relaxation time collision

It is now widely-known that the use of the SRT scheme introduced in equation (1), though being computationally cheap, is the source of numerical oscillations in the pressure and velocity field. Such oscillations may specially end up in complete divergence in the case of very low viscosities, as may occur in the gas phase in multiphase flows. The destructive influence of the SRT scheme on the magnitude of the spurious velocities is also well studied in the works of Yu and Fan [37] and Fakhari and Lee [9]. Such unfavourable effects emerge from the fact that in the single relaxation time collision, all the moments of the distribution function are forced to relax towards equilibrium through the same relaxation time τ which is a function of viscosity ν . A well-established remedy is to let the different moments of the flow relax through a multiple relaxation time (MRT) mechanism. To this end, one has to first transform the distribution functions from the phase space $\mathbf{g} = (g_0, \dots, g_8)^T$ to their hydrodynamic counterparts in the moments space $\hat{\mathbf{g}}$ as

$$\hat{\mathbf{g}} = \mathbb{M} \mathbf{g} = (\rho, \eta, \eta^2, \rho u_x, q_x, \rho u_y, q_y, \gamma_{xx}, \gamma_{yy})^T \quad (31)$$

where the transformation matrix \mathbb{M} for the D2Q9 model in two dimensions is given [17] as:

$$\mathbb{M} = \begin{bmatrix} 1 & 1 & 1 & 1 & 1 & 1 & 1 & 1 & 1 \\ -4 & -1 & 2 & -1 & 2 & -1 & 2 & -1 & 2 \\ 4 & -2 & 1 & -2 & 1 & -2 & 1 & -2 & 1 \\ 0 & 1 & 1 & 0 & -1 & -1 & -1 & 0 & 1 \\ 0 & -2 & 1 & 0 & -1 & 2 & -1 & 0 & 1 \\ 0 & 0 & 1 & 1 & 1 & 0 & -1 & -1 & -1 \\ 0 & 0 & 1 & -2 & 1 & 0 & -1 & 2 & -1 \\ 0 & 1 & 0 & -1 & 0 & 1 & 0 & -1 & 0 \\ 0 & 0 & 1 & 0 & -1 & 0 & 1 & 0 & -1 \end{bmatrix} \quad (32)$$

The new moments in equation (31) are the kinetic energy η , momentum flux q and the diagonal components of the surface tension tensor γ . Considering the general relaxation operator Λ in the phase space in equation (38), the transformed relaxation matrix $\hat{\Lambda} = \mathbb{M}\Lambda\mathbb{M}^{-1}$ has the diagonal form

$$\hat{\Lambda} = \text{diag}\{s_0, s_1, s_2, s_3, s_4, s_5, s_6, s_7, s_8\}. \quad (33)$$

The moments \hat{g}_k could then get relaxed through their individual relaxation times using s_k . In practice, one carries out the collision part of the LBM in the moment space and then uses the inverse transform \mathbb{M}^{-1} to obtain the post-collision values g_k so as to perform the streaming part in the phase space

$$g_k(x + e_k\Delta t, t + \Delta t) = g_k(x, t) - \mathbb{M}^{-1} \left[\sum_j \hat{\Lambda}_{k,j} (\hat{g}_j(x, t) - \hat{g}_j^{eq}(x, t)) + (I - \frac{1}{2}\hat{\Lambda}_{k,j}) \hat{S}_j(x, t) \right] \quad (34)$$

A general choice for the relaxation times s_k , tuned for stability is discussed in [17] and further investigated by [9] and [37] for multiphase flows. Eventually, a primary setting is suggested as

$$\hat{\Lambda} = \text{diag}\{1, s_1, s_2, 1, s_4, 1, s_4, 1/\tau, 1/\tau\}. \quad (35)$$

where the surface tension relaxations s_7, s_8 are related to the viscosity through $\tau = 3(\bar{\mu}/\bar{\rho}) + 0.5$. The general rule of thumb for s_1, s_2 and s_4 is to keep their values near 1.0. However, since s_1 is associated with the kinetic energy mode, its selection strongly affects the obtained velocity field. We will discuss in section 4 that setting $s_1 < 0.5$, gives the optimal results in the problems concerned in this paper.

3 Solving the level set equation

In order to solve the level set equation (9) for capturing the interface, we use the following second order Runge-Kutta time integration. Assuming that ϕ_{ij}^n and \mathbf{u}_{ij}^n are the values of the level set function and the velocity at node (i, j) and time n , we have

$$\phi_{ij}^* = \phi_{ij}^n - \Delta t \mathbf{u}_{ij}^n \nabla \phi_{ij}^n \quad (36)$$

which gives the predictive value of ϕ_{ij}^* , followed by a correction solution

$$\phi_{ij}^{n+1} = \phi_{ij}^n - \frac{\Delta t}{2} (-\mathbf{u}_{ij}^n \nabla \phi_{ij}^n + \mathbf{u}_{ij}^n \nabla \phi_{ij}^*). \quad (37)$$

To discretize the convective term $\mathbf{u}_{ij} \nabla \phi_{ij}$, we use the weighted essentially non-oscillatory (WENO) scheme as described in [25] which extends the first-order accurate upwind differencing to fifth-order spatial accuracy based on the smoothest possible interpolation for the function ϕ . It is worth noting that although the level set function is generally known to have smooth variations in the computational field, the use of the WENO

scheme ensures that the interface is accurately convected in the case that sharp kinks or edges of the bubble might locally disturb the signed distance property of the level set functions which eventually produces steep changes in the value of ϕ . As such local effects could only be moderated to some extent by reinitializing the level set function (see section 3.1), it is reasonable to employ the smoothest approximation for the spacial derivatives of ϕ . We note that at this stage of the work the same computational mesh as for the LBM is used for the discretization of the level set equation, meaning that $\Delta t = 1, \Delta x = 1$. Since the velocities obtained from LBM are in the incompressible range of $u_{max} \ll 1$, one could be sure that the CFL condition of $\Delta t < \Delta x/u$ is always satisfied for this choice of $\Delta t, \Delta x$.

3.1 Level set reinitialization

As the solution of equation (9) advances in time, the level set function deviates from the signed distance property as initially assumed in section 2.2. Therefore, one needs to reinitialize the level set function to be close to the signed distance function. At this stage of the work, a brute force method is employed to find ϕ_{dist} which calculates the minimum distances from the nodes to the linear edges which approximate the interface [?]. Eventually, we use the following smoothed reinitialization, previously introduced in [?]

$$\phi_{new} = \alpha\phi_{dist} + (1 - \alpha)\phi_{old} \quad (38)$$

where $0 \leq \alpha \leq 1$, and $\alpha = 0$ means no reinitialization, while $\alpha = 1$ results in full redistancing. Care must be taken to prevent the $\phi = 0$ level set from changing position and thus loss of mass during the interface reconstruction. Our numerical experiments suggest that using $0.1 \leq \alpha \leq 0.15$ leads to minimum mass loss and best accuracy in capturing the interface.

4 Numerical results

In all the numerical tests in this section we make use of the two numerical discretization approaches described in section 2.3, namely Approach-1 and Approach-2; Approach-1 refers to adopting the simple central differencing for all the gradients including the pressure, whereas Approach-2 uses the averaged directional formulation for the gradient of pressure and the central differencing for the rest of the gradients.

Since we eventually aim to compare our rising bubble simulations against the FEM solutions by Hysing et al. [16], we choose the parameter settings as defined for the two rising bubble test-cases in that work and apply the corresponding LB-converted parameters to both static and rising bubble simulations in the present study. A summary of the configurations in LBM units is given in Table 1.

Table 1: Physical parameters and dimensionless numbers for test case 1 and 2, applied to static and rising bubble

test case	ρ_l	ρ_g	μ_l	μ_g	Re	EO	ρ_l/ρ_g	μ_l/μ_g
Test case 1	10	1	0.1	0.01	35	10	10	10
Test case 2	500	0.5	2	0.02	35	125	1000	100

LBM's density and viscosity could be chosen to tune the relaxation values s_7, s_8 to achieve higher stability, while the rest of the parameters, e. g. surface tension σ , gravity \mathbf{g} and time t have to be calculated in accordance to the non-dimensional numbers e. g. EO and Re as well as the non-dimensional time T which are defined as below

$$Eo = \frac{4\rho_l \mathbf{g} r_0^2}{\sigma} \quad (39)$$

$$Re = \frac{\rho_l \sqrt{\mathbf{g}} (2r_0)^{3/2}}{\mu_l} \quad (40)$$

$$T = \sqrt{\frac{\mathbf{g} t}{r_0}} \quad (41)$$

where r_0 is the bubble radius and is measured as the number of lattice units which the radius occupies.

4.1 Static bubble

We start our validation tests with the static bubble problem. The bubble has the radius of $r_0 = 0.25$ and an interface thickness of $\varepsilon = 0.05$, placed in the centre of a 1×1 computational domain with periodic boundary conditions on all the entities. We aim to check the solutions against the Laplace law which, for a two dimensional static bubble, describes the pressure difference due to the surface tension effect as

$$P_{in} - P_{out} = \frac{\sigma}{r_0}. \quad (42)$$

We will also examine the magnitudes of the spurious velocities which usually form around the interface as a result of the force discretization error and lack of isotropy [18, 37].

The first test mimics the parameter configuration for test case 1 in Table 1. The simulation is run up to $t = 3$ (corresponding to $T = 3.43$) and we use both Approach 1 and 2 as well as the MRT-based Shan-Chen diffused interface LB model with eight order force calculations [37]. Table 2 compares the error in the pressure as well as the spurious velocity on different mesh levels. One could see that the maximum of the spurious velocity is in average improved upon the Shan-Chen model by one and two orders of magnitude using Approach 1 and 2 of the coupled LBM-Level set scheme, respectively. Unlike the LB model where the velocity error decreases by refining the lattice, the Shan-Chen model tends to increase the spurious velocities since the actual interface thickness becomes thinner, making the jumps more sharp and hence the force approximation less accurate.

It is also worth nothing that the higher isotropy in Approach 2 has resulted in one order of magnitude lower spurious velocity as compared to Approach 1. Nevertheless, the rather low density and viscosity differences in this case introduce no major error in recovering the pressure, and the errors in the Laplace equation are of the same level using both approaches.

Next we increase the density and viscosity ratios to 1000 and 100 respectively in accordance to parameters for the test case 2. As the Shan-Chen model is not capable to incorporate such high density/viscosity differences into its two-component variant, we only present the results using the coupled LBM-level set scheme. As depicted in Table 3, Approach 1 almost fails to recover the correct pressure even up to a lattice as fine as $h = 1/160$ with a pressure error of 13%, whereas the corresponding error for Approach 2 is less than 1% at nearly one order of magnitude lower spurious velocities.

Figure 1 provides the pressure profile obtained using both discretization approaches on different lattice levels. The simple central differencing approach leads to an overly-smoothed pressure profile which could not reach the correct values of pressure even up to $h = 1/160$ as required by the Laplace law. In contrast, the averaged directional technique of Approach 2 has succeeded in preserving the sharp pressure jump across the interface and the pressure values arrive at the expected levels in a length of almost 2ε .

Table 2: pressure and velocity errors for the static bubble test case 1 using different lattice levels

$1/h$	40	80	160	320
Shan-Chen LB Model				
U_{max}	6.5e-5	1.4e-4	3.00e-4	6.24e-4
$ \Delta P - \sigma/r_0 /(\sigma/r_0)$	0.0453	0.0172	0.0017	0.0023
LBM-Level Set, Approach 1				
U_{max}	5.8e-5	3.00e-5	9.8e-6	7.4e-6
$ \Delta P - \sigma/r_0 /(\sigma/r_0)$	0.0108	0.0126	0.0087	0.0058
LBM-Level Set, Approach 2				
U_{max}	1.93e-5	8.2e-6	4.6e-6	2.6e-6
$ \Delta P - \sigma/r_0 /(\sigma/r_0)$	0.0277	0.0147	0.0086	0.0060

Table 3: pressure and velocity errors for the static bubble test 2 using different lattice levels

$1/h$	40	80	160	320
LBM-Level Set, Approach 1				
U_{max}	4.7e-6	5.0e-6	3.0e-6	2.1e-6
$ \Delta P - \sigma/r_0 /(\sigma/r_0)$	0.7520	0.4250	0.1331	0.0249
LBM-Level Set, Approach 2				
U_{max}	5.7e-6	4.1e-6	8.4e-7	3.6e-7
$ \Delta P - \sigma/r_0 /(\sigma/r_0)$	0.1611	0.0211	0.0080	0.0060

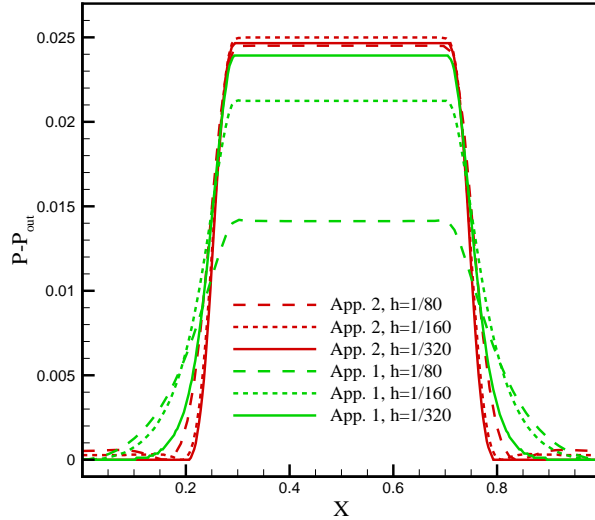


Fig. 1: Pressure profile for the static bubble test 2

4.2 Rising bubble

The rising bubble problem consists of a bubble of radius $r_0 = 0.25$ placed in a rectangular domain of size 1×2 as illustrated in Figure 2. The no-slip boundary condition is considered for the horizontal walls using the second order bounceback scheme [36], while we impose periodic boundary conditions on the vertical boundaries which, in this particular geometry, implies the slip boundary condition ($\mathbf{u} \cdot \mathbf{n} = 0$) as in [16]. Initially the bubble is stationary and is then allowed to rise by adding the buoyancy force $F_b = \mathbf{g}(\rho(\phi) - \rho_l)$ to $\bar{F}/\rho(\phi)$ in equation (18). which only acts on the lighter fluid inside the bubble. Two test cases are carried out according to the configurations given at the beginning of section 4. For both test cases the interface thickness is set to $\varepsilon = 0.03$ and the level set is reinitialized every $N = 5$ time steps for the base mesh of

$h = 1/40$ and N would be increased by a factor of 4 by refining the lattice spacing from h to $h/2$ (since $\Delta t \propto h^2$ in LBM).

In order to provide a quantitative insight into the bubble dynamics, the temporal values of the different bubble metrics are considered as benchmark quantities and will be calculated in time for each test case. Here we use the temporal values of the bubble centroid position y_c , bubble rise velocity \mathbf{u}_c and its circularity \mathcal{c} defined as

$$y_c = \frac{\int_{\Omega_b} y dx}{\int_{\Omega_b} 1 dx} \quad (43)$$

$$\mathbf{u}_c = \frac{\int_{\Omega_b} \mathbf{u} dx}{\int_{\Omega_b} 1 dx} \quad (44)$$

$$\mathcal{c} = \frac{P_a}{P_b} = \frac{\text{perimeter of area-equivalent circle}}{\text{perimeter of bubble}} = \frac{\pi d_a}{P_b} \quad (45)$$

where Ω_b refers to the subspace of the lattice cells with coordinate $\mathbf{x} = (x, y)$ where $\phi(x, y) < 0$, i. e. they fall inside the bubble.

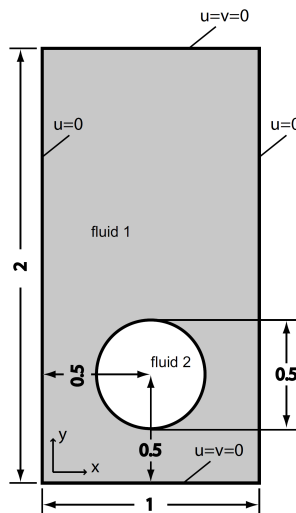


Fig. 2: Initial configuration and boundary conditions for the rising bubble problem [16]

4.2.1 Test case 1

In the first test known as *test case 1* in [16], we choose the corresponding parameters as in Table 1 where the density and viscosity ratios are both set to 10. As the time elapses the bubble is expected to gain a stable ellipsoidal shape. An illustration of the time evolution of the bubble shape is depicted in Figure 3 for a lattice of $h = 1/160$ using the Shan-Chen LBM, Approach 1 and 2 of the coupled scheme and the finite element solution obtained by the FeatFlow package [16]. While the interface obtained by the LBM-Level Set scheme closely resembles that by the FeatFLOW, the Shan-Chen model produces more noticeable discrepancies from the reference shapes.

The convergence behaviour of the coupled scheme with Approach 2 for the eventual interface shape is illustrated in Figure 4. The convergence trend is further examined in time for the bubble quantities in Figure

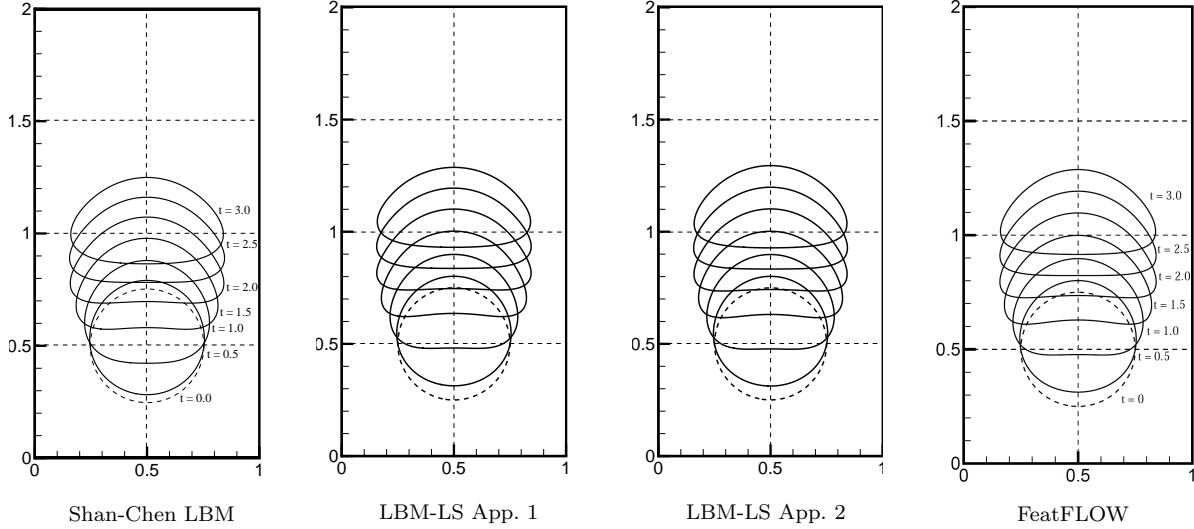


Fig. 3: Time evolution of the bubble shape for the Test Case 1

5. The differences between the curves of $h = 1/80$, $h = 1/160$ and $h = 1/320$ are quite small, while the curve of the coarsest lattice of $h = 1/40$ has clear deviation from the fine grid solutions and experiences difficulty in retaining the ellipsoidal shape of the bubble after $t = 2$ as reflected in the circularity curves. The main reason is that the quality of our interface reconstruction degrades largely at coarser lattices which also provokes intermittent jumps in the circularity curve due to the periodic reinitialization of a weakly reconstructed interface. Table 4 contains the time-integrated errors in the rise velocity in different norm spaces measured relative to the reference lattice of $h = 1/320$. The calculated rates of convergence (from $h/2$ to h) (ROC) show that the overall accuracy of the coupled scheme in L_1 and L_2 norm spaces is in between 1.5 and 2 which confirms the second order accuracy in both Approach 1 and 2.

Finally, Figure 6 shows a quantitative comparison between different schemes on the finest level of $h = 1/320$. Again, a very close agreement is discerned between the solutions from the coupled LBM-level set scheme (using both approaches) and those produced by FeatFLOW. Although the Shan-Chen model is able to capture the overall temporal trend, it exhibits apparent deviations especially in the bubble velocity, where the velocities are in average lower than the reference solution. As also pointed out for the static case, Approach 1 is successful in recovering the correct pressure field for such moderate density and viscosity differences and therefore we did not expect it to introduce any noticeable error in the dynamic test as well.

Table 4: Errors in the bubble rise velocity and the rates of convergence (ROC) for the test case 1

LBM-Level Set, Approach 1						
$1/h$	$\ e_1\ $	ROC_1	$\ e_2\ $	ROC_2	$\ e_\infty\ $	ROC_∞
40	0.076750		0.149206		0.177204	
80	0.028549	1.426712	0.053590	1.477261	0.055123	1.684686
160	0.007367	1.954169	0.013609	1.977321	0.024643	1.161464
LBM-Level Set, Approach 2						
$1/h$	$\ e_1\ $	ROC_1	$\ e_2\ $	ROC_2	$\ e_\infty\ $	ROC_∞
40	0.096958		0.051369		0.046389	
80	0.042549	1.188226	0.021663	1.245647	0.020337	1.189679
160	0.013890	1.615036	0.000692	1.644344	0.000757	1.424072

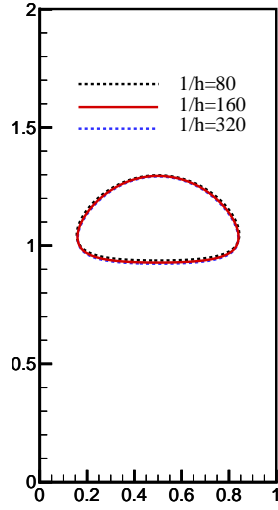


Fig. 4: Bubble interface shape at $t = 3$ using different lattice levels

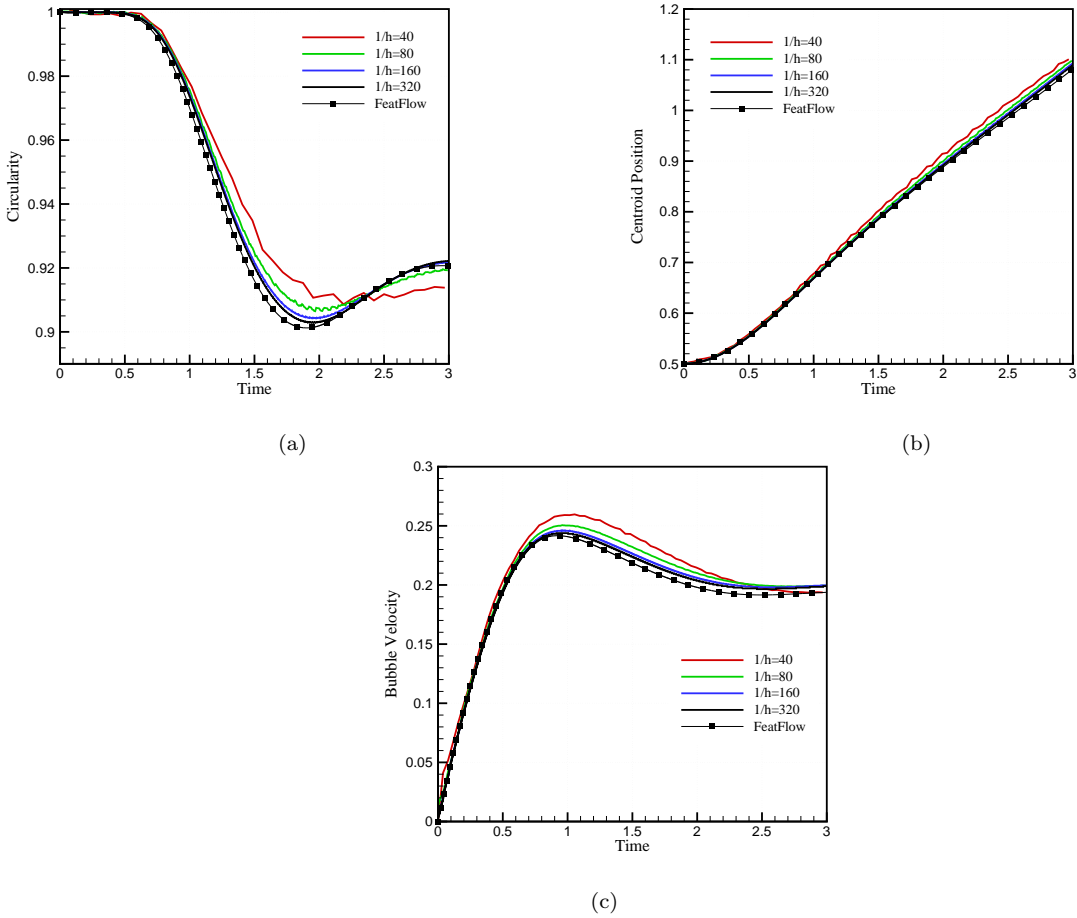


Fig. 5: Temporal values of bubble metrics using the coupled LB-level set scheme with Approach 2 on different lattice levels for the test case 1, (a) bubble circularity (b) centroid position (c) rise velocity

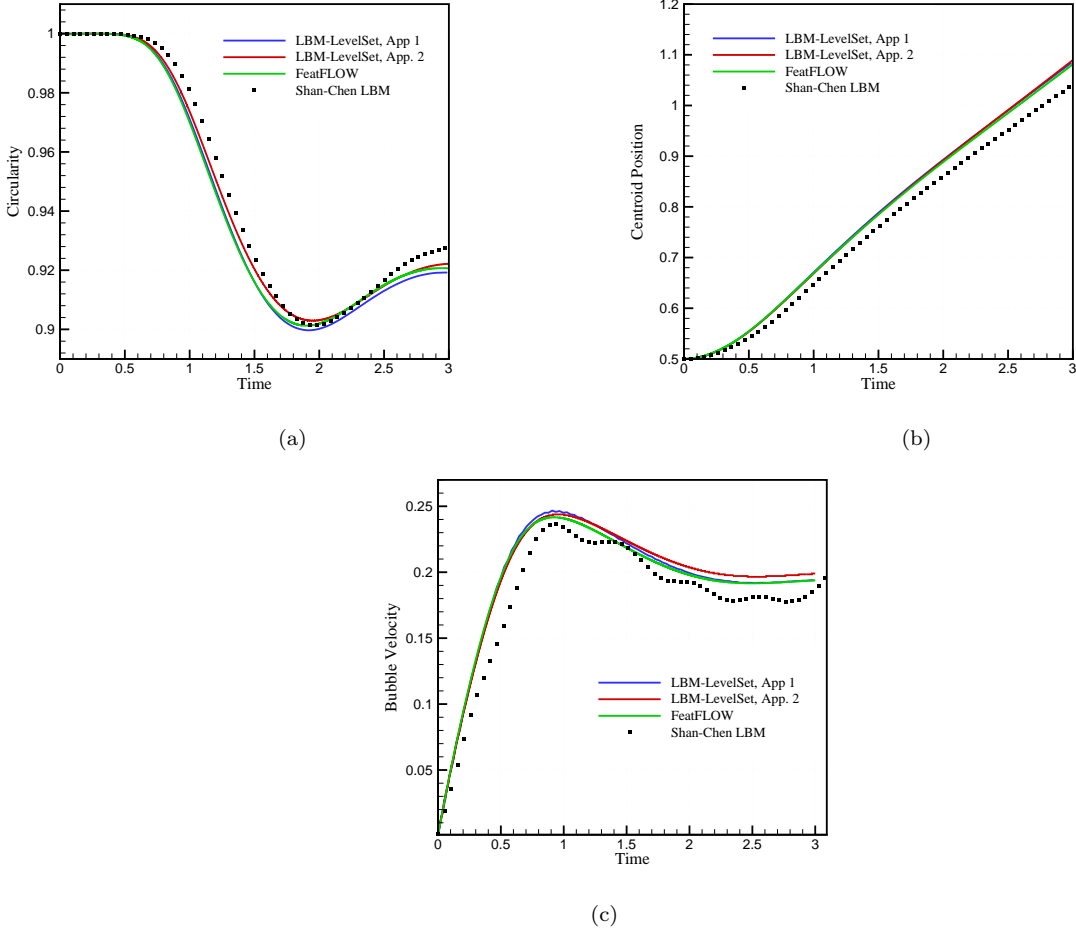


Fig. 6: Temporal values of bubble metrics using different numerical schemes for the test case 1, (a) bubble circularity (b) centroid position (c) rise velocity

4.2.2 Test case 2

In the second test case we increase the bubble density and viscosity ratios to more demanding values of 1000 and 100 respectively while the rest of the parameters are chosen as in Table 1. By assuming the same Re number as in the test case 1, the bubble velocity is almost kept constant. However, the increase in the Eo number from 10 in the previous test to 125 means that the surface tension is decreased. According to the bubble shape map, proposed by Clift et al. [7], the bubble is expected to attain the shape of a dimpled cap. As illustrated in Figure 7 (for a mesh of $h = 1/160$), the coupled LB-level set scheme is successful in recovering the time evolution of the bubble shape which closely resembles the one predicted by the FeatFLOW finite element solution in [16]. One could also see that the level set equation discretized with the WENO finite differencing is capable of resolving very sharp corners and thin filaments as necessary for such a high Eo number simulation. We note that the Shan-Chen model could not be used in this test case, as also pointed out for the high density ratio static bubble test case.

In fact the major distinction between different approaches, seen in Figure 7, is the separation of the trailing edge filaments predicted by FeatFLOW, whereas they remain attached to the bulk body of the cap-shaped bubble in the LBM calculations. The separation could be a result of special parameterization in the level set module or the interface reconstructions techniques used by FeatFLOW. In fact, there exists no reference

solution for this test case after $t = 2$ since other FEM solutions e. g. the FreeLIFE package [8] do not report such a phenomenon for the same benchmark. This could be examined quantitatively using the temporal values of bubble metrics as in Figure 8 where the agreement between the circularity values given by FeatFLOW, FreeLIFE and the coupled LBM-level set breaks up at around $t = 2.3$ and one could spot an abrupt jump of the circularity in the curve obtained by FeatFLOW in Figure 8. Nevertheless, a fairly good agreement keeps up for the centroid position up to $t = 2$. For the rise velocity the agreement stays up to $t = 1$ where the deviation from the FEM solutions grows slowly up to $t = 3$. Such a deviation could most probably be associated with the relatively larger pressure gradients produced by the motion of the bubble in the case of large density differences which consequently affects the velocity field. In fact the approximation of the pressure by the ideal gas EOS (6) is not very accurate to recover such large dynamic pressure gradients.

Another key observation is that the use of the coupled scheme with force discretization of Approach 1 for this test case would result in totally incorrect predictions of the bubble quantities as well as its shape (as depicted in Figure 9 for different lattice levels). This was rather expected from the high pressure errors emerging in the high density ratio static bubble test. The large deviations from the reference solutions are thus due to the errors in the pressure field which tend to grow drastically on coarser lattices. In contrary, Approach 2 manifests a smooth convergence from coarser lattices to finer ones in both the benchmark quantities (as shown in Figure 10) and the interface shape. The overshoots of the rise velocity at the early times is again produced by the high dynamic pressure gradient which forms around the bubble as the bubble starts to rise in the surrounding stationary liquid. Nevertheless, using finer lattices eventually enhances the pressure gradient accuracy to some extent and removes the starting overshoots.

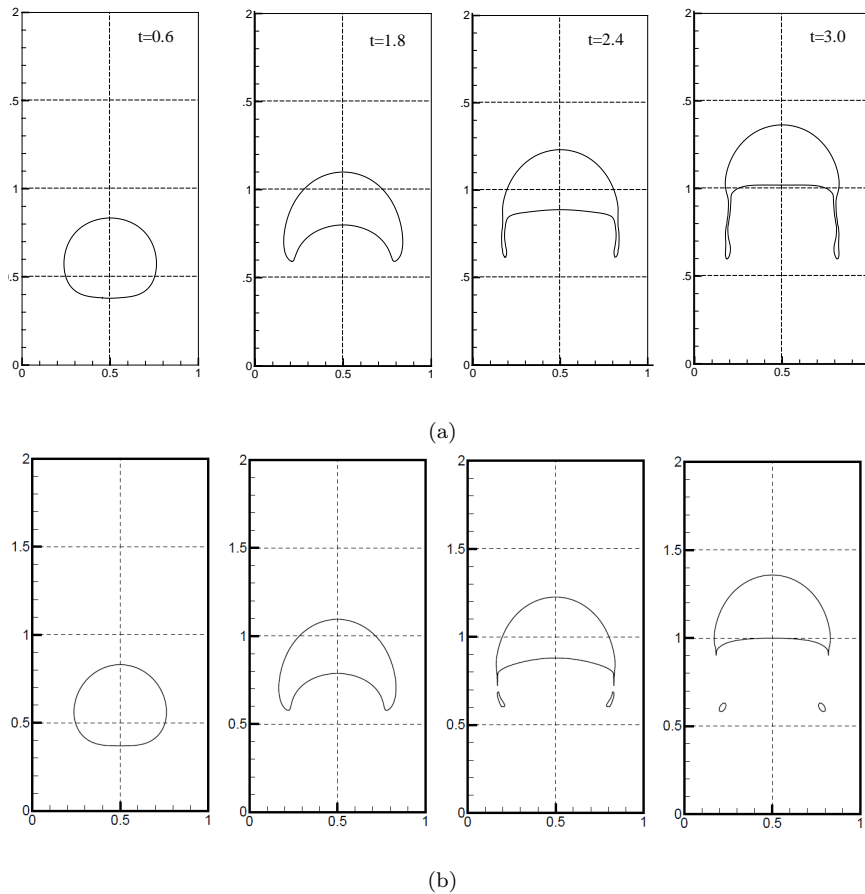


Fig. 7: Time evolution of the bubble in the test case 2 for $h = 1/160$ using (a) LB-level set scheme Approach 2 (b) FeatFLOW

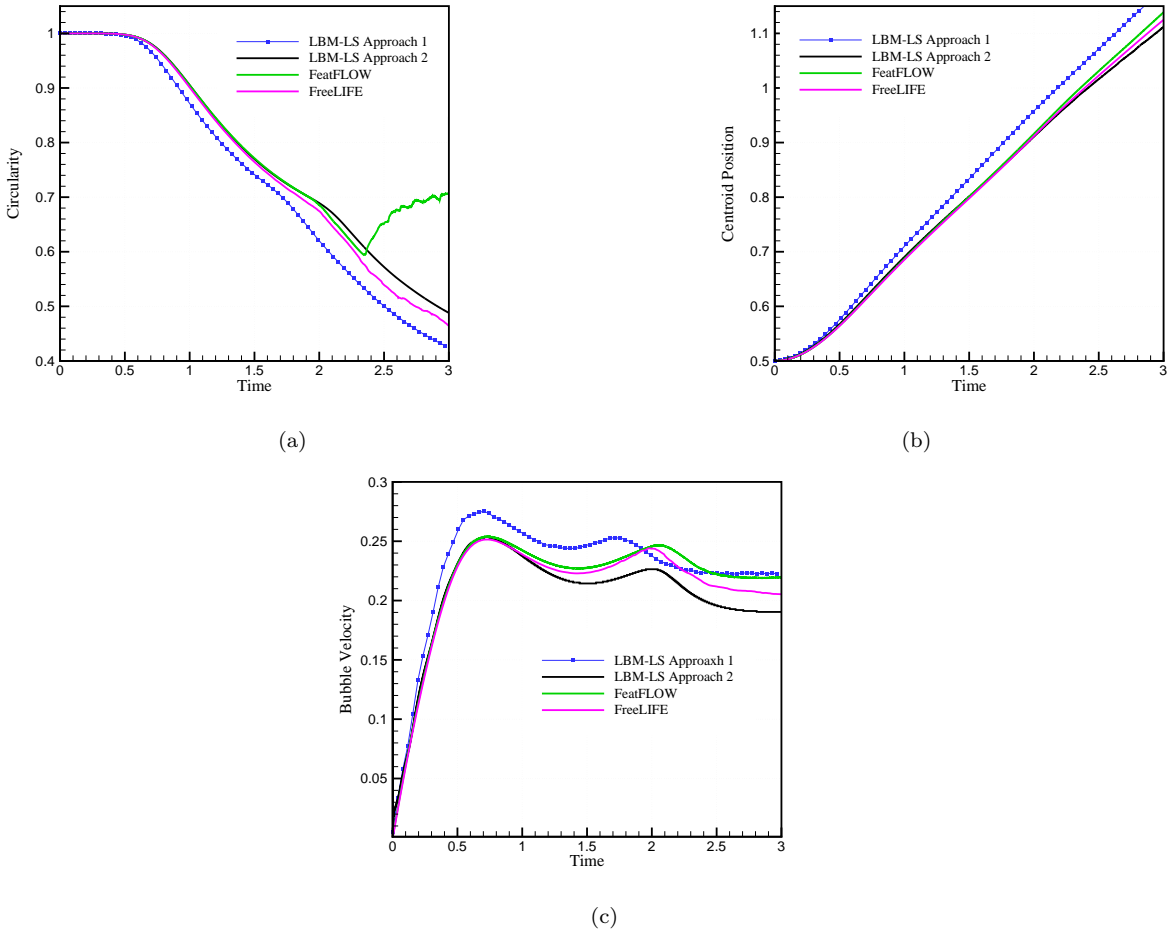


Fig. 8: Temporal values of the bubble quantities using different numerical schemes for test case 2, (a) bubble circularity (b) centroid position (c) rise velocity

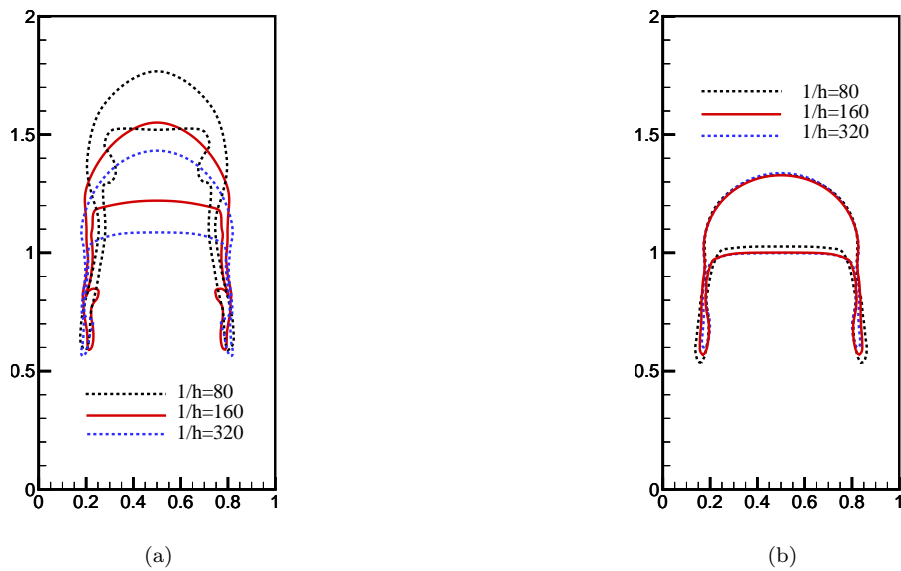


Fig. 9: Bubble interface for test case 2 at time $t = 3$ on different lattice levels using the LB-level set scheme (a) Approach 1 (b) Approach 2

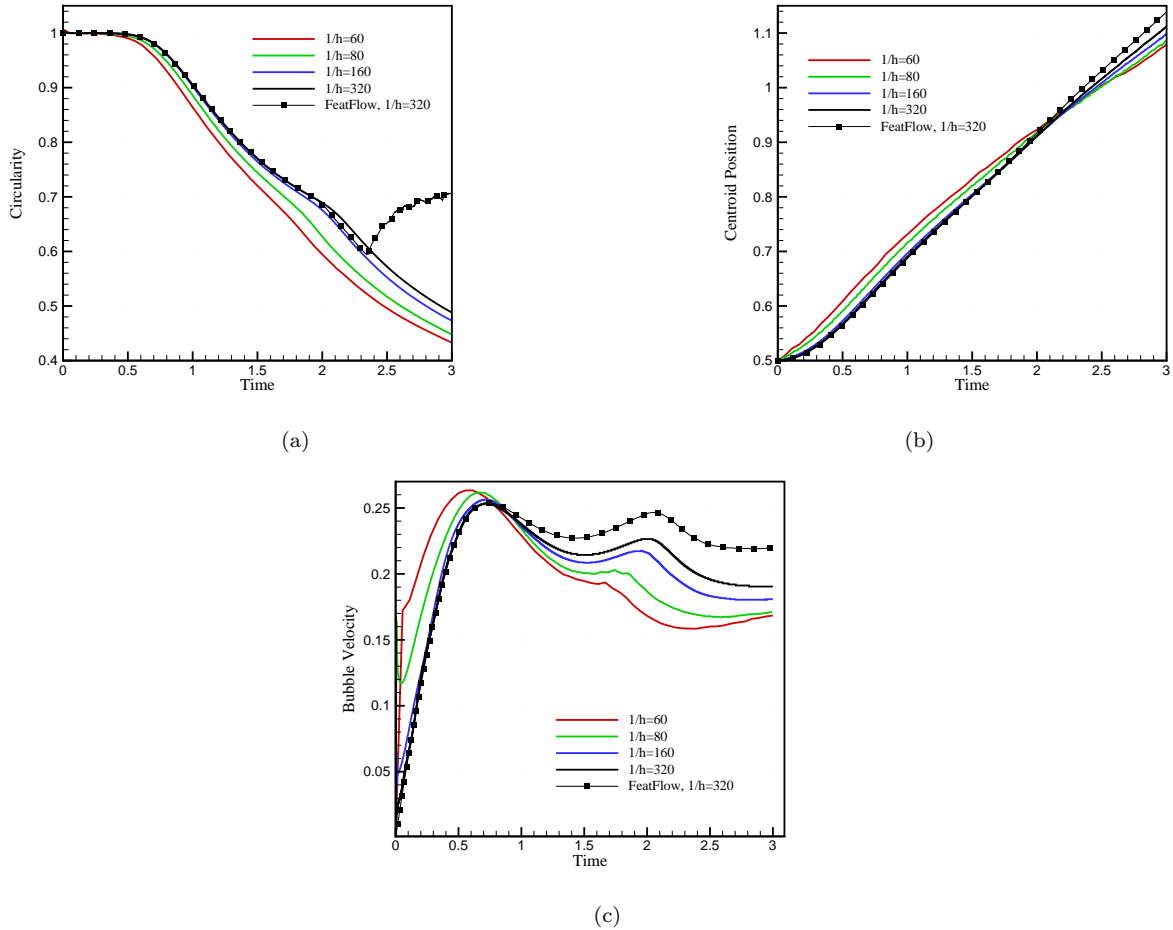


Fig. 10: Temporal values of the bubble quantities for test case 2 on different lattice levels using the coupled LB-level set scheme with Approach 2, (a) bubble circularity (b) centroid position (c) rise velocity

4.3 Relaxation time calibration

As previously mentioned in section 3, one has to take special care in choosing the right relaxation value s_1 for the energy mode η . In order to investigate the effect of different values of s_1 on the numerical results, in Figure 11a we have measured the temporal values of the mean kinetic energy $\bar{\eta}$ in the static bubble problem at density and viscosity ratio equal to 1000 and 100 respectively. It is evident from Figure 11(a) that by over-relaxing the s_1 values to be larger than 1, the kinetic energy experiences large oscillations before converging to its final level. To dissipate the oscillations one may try to under-relax the energy mode using $s_1 < 1$ such that the convergence becomes fairly smooth for $s_1 = 0.3$. The observation is also prevalent in the dynamic problem of the rising bubble test case 2 as depicted in Figure 11(b) for the bubble rise velocity. It is seen that the rise velocity would not become smooth unless choosing to under-relax the energy moment. Such a phenomenon is believed to become more pronounced and effective in dynamic problems as the Eu number increases, i. e. the inertial effects may dominate the surface tension forces. A similar deduction is pointed out in [9] for the MRT implementation of the chemical potential model where the use of $s_1 = 0.5$ for bubble problems and $s_1 = 1.0$ for Kelvin-Helmholtz instability simulations has resulted in higher stability

properties. This is, however, in contrast with the general advise in the literature to have $1.5 < s_1 < 1.7$ [17, 24, 37].

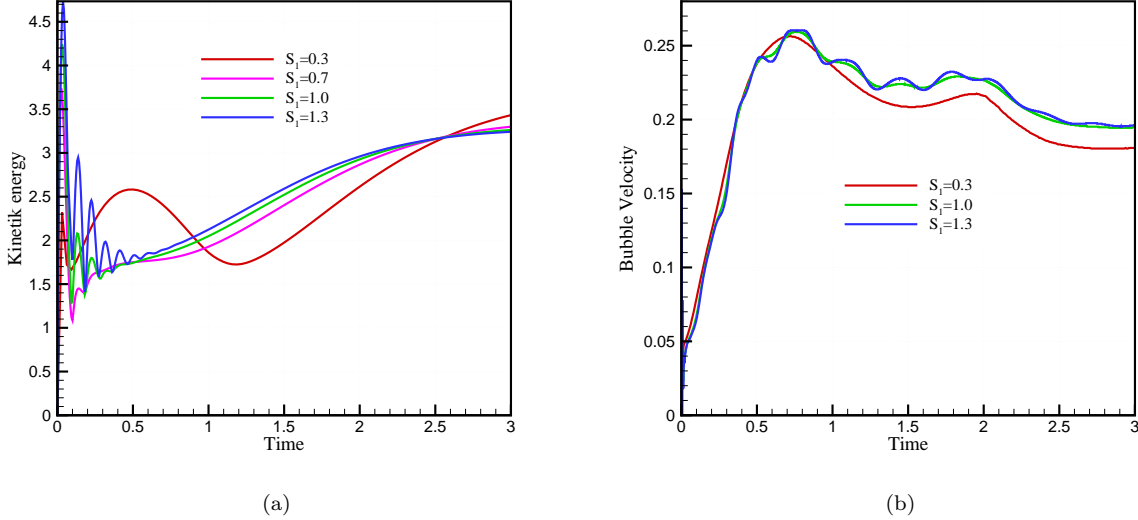


Fig. 11: Effect of choosing different relaxation values s_1 on (a) static bubble kinetic energy (b) the rise velocity of the rising bubble test case 2. In both cases the lattice spacing is $h = 1/160$

4.3.1 Summary and conclusions

A second order coupled LB-level set scheme was designed for multiphase flow problems based on the one-fluid formulation of the governing equations. The averaged directional pressure force discretization enables us to capture the correct pressure field for static and rising bubble problems with density and viscosity ratios as high as 1000 and 100, respectively. In particular, qualitative and quantitative benchmarking against the finite element solution of rising bubble problems (as available in [16]) proves the accuracy of the coupled scheme at both moderate and high density and viscosity ratios. While the present model outperforms the classical Shan-Chen model in the static and rising bubble tests, it removes the Shan-Chen model limitation to low density or viscosity ratios. The use of the one-fluid formulation further eliminates the need to impose explicit boundary conditions on the interface or to have different lattice spacings in the case of large viscosity differences as necessary in [35]. Moreover, it requires less computational effort as compared to the chemical potential LB models e. g. [20] since it includes less derivatives in the force evaluation and replaces the second D2Q9 LBE for interface capturing in [20] with a 2D PDE for solving the level set function. We note that since the model is originally designed based on the ideal gas EOS to evaluate the pressure, its application to problems with large dynamic pressure gradients may result in non-accurate pressure and velocity fields. As a remedy, one could exclude the ideal gas contribution from the total pressure and redesign the LBE to solve for the dynamic pressure as suggested by [12].

The level set interface capturing is demonstrated to be a promising tool for capturing complex bubble deformations at high EO numbers when being added to a lattice Boltzmann flow solver. As this study was mainly focused on implementing the coupled approach and evaluating the overall performance and accuracy, we have employed the most basic numerical tools available as reinitialization and surface reconstruction modules which might be neither the most computationally efficient nor numerically accurate. Yet, we expect a significant improvement in the interface capturing quality through employing more sophisticated reinitialization schemes e. g. the fast marching method or make use of the polynomial recovery approximations for evaluating the surface normals and curvature.

The level set equation is currently using an identical mesh spacing as for the LBM. However, since one is only interested to solve the level set function accurately in the vicinity of the interface, the use of a fine mesh could be avoided in the far field by employing a separate, locally refined mesh for the level set, resulting in considerable savings in the computational cost. An even further advanced technique, widely used in Navier-Stokes-based solvers, is to solve the level set equation using finite element schemes on unstructured meshes adaptively refined around the interface which provide higher interface resolutions, yet at the price of sacrificing the scalability of parallel implementations.

Finally, considering the renowned capability of LB solutions for parallelization and the fact that the extension of the method to three dimensions is straightforward, the authors believe that the present coupled scheme could show off its competitive functionality by benefiting from parallel implementation, and in particular GPUs for large scale three dimensional multiphase flow simulations. A major milestone in this regard would be to minimize the computational overhead due to interface reinitialization and reconstruction. Early results regarding the use of more robust pressure approximations, advanced numerical tools for the interface reconstruction, and finally efficient parallel implementation are very promising and are subject to our future publications.

Acknowledgements

This work was supported by the the German Graduate School of Energy Efficient Production and Logistics at TU Dortmund.

References

- [1] Exa powerflow software, 2014.
- [2] Openlb software, 2014.
- [3] Palabos software, 2014.
- [4] J. Bao and L. Schaefer. Lattice boltzmann equation model for multi-component multi-phase flow with high density ratios. *Applied Mathematical Modelling*, 37(4):1860–1871, 2013.
- [5] J. Becker, M. Junk, D. Kehrwald, G. Thmmes, and Z. Yang. A combined lattice bgk/level set method for immiscible two-phase flows. *Computers and Mathematics with Applications*, 58(5):950–964, 2009.
- [6] S. Chen and G.D. Doolen. Lattice boltzmann method for fluid flows. *Annual Review of Fluid Mechanics*, 30:329–364, 1998. cited By (since 1996)2775.
- [7] Grace J. R. Clift, R. and M. E. Weber. *Bubbles, Drops and Particles*. Academic Press, New York, First edition, 1978.
- [8] D.A. Di Pietro, S. Lo Forte, and N. Parolini. Mass preserving finite element implementations of the level set method. *Applied Numerical Mathematics*, 56(9):1179–1195, 2006.
- [9] A. Fakhari and T. Lee. Multiple-relaxation-time lattice boltzmann method for immiscible fluids at high reynolds numbers. *Physical Review E - Statistical, Nonlinear, and Soft Matter Physics*, 87(2), 2013.
- [10] U. Frisch, D. d’Humières, B. Hasslacher, P. Lallemand, Y. Pomeau, and J. P. Rivet. Lattice gas hydrodynamics in two and three dimensions. *Complex Syst.*, 1:649–707, 1987.
- [11] X. He, S. Chen, and G.D. Doolen. A novel thermal model for the lattice boltzmann method in incompressible limit. *Journal of Computational Physics*, 146(1):282–300, 1998.
- [12] X. He, S. Chen, and R. Zhang. A lattice boltzmann scheme for incompressible multiphase flow and its application in simulation of rayleigh-taylor instability. *Journal of Computational Physics*, 152(2):642–663, 1999.
- [13] X. He and L.-S. Luo. A priori derivation of the lattice boltzmann equation. *Physical Review E - Statistical Physics, Plasmas, Fluids, and Related Interdisciplinary Topics*, 55(6 SUPPL. A):R6333–R6336, 1997.
- [14] X. He, X. Shan, and G.D. Doolen. Discrete boltzmann equation model for nonideal gases. *Physical Review E - Statistical Physics, Plasmas, Fluids, and Related Interdisciplinary Topics*, 57(1):R13–R16, 1998.

- [15] S. Hysing. *Numerical simulation of immiscible fluids with FEM level set techniques*. PhD thesis, Technische Universität Dortmund, December 2007.
- [16] S. Hysing, S. Turek, D. Kuzmin, N. Parolini, E. Burman, S. Ganesan, and L. Tobiska. Quantitative benchmark computations of two-dimensional bubble dynamics. *International Journal for Numerical Methods in Fluids*, 60(11):1259–1288, 2009.
- [17] P. Lallemand and L.-S. Luo. Theory of the lattice boltzmann method: Dispersion, dissipation, isotropy, galilean invariance, and stability. *Physical Review E - Statistical Physics, Plasmas, Fluids, and Related Interdisciplinary Topics*, 61(6 B):6546–6562, 2000. cited By (since 1996)528.
- [18] T. Lee and P.F. Fischer. Eliminating parasitic currents in the lattice boltzmann equation method for nonideal gases. *Physical Review E - Statistical, Nonlinear, and Soft Matter Physics*, 74(4), 2006.
- [19] T. Lee and P.F. Fischer. A lattice boltzmann equation method without parasitic currents and its application in droplet coalescence. volume 1 SYMPOSIA, pages 675–681, 2006.
- [20] T. Lee and C.-L. Lin. A stable discretization of the lattice boltzmann equation for simulation of incompressible two-phase flows at high density ratio. *Journal of Computational Physics*, 206(1):16–47, 2005.
- [21] L.-S. Luo. Unified theory of lattice boltzmann models for nonideal gases. *Physical Review Letters*, 81(8):1618–1621, 1998.
- [22] M. Mehravaran and S. Kazemzadeh Hannani. Simulation of buoyant bubble motion in viscous flows employing lattice boltzmann and level set methods. *Scientia Iranica*, 18(2):231 – 240, 2011.
- [23] M. Mehravaran and S.K. Hannani. Simulation of incompressible two-phase flows with large density differences employing lattice boltzmann and level set methods. *Computer Methods in Applied Mechanics and Engineering*, 198(2):223–233, 2008.
- [24] S. Mukherjee and J. Abraham. A pressure-evolution-based multi-relaxation-time high-density-ratio two-phase lattice-boltzmann model. *Computers and Fluids*, 36(6):1149–1158, 2007.
- [25] Fedkiw R. Osher, S. *Level Set Methods and Dynamic Implicit Surfaces*. Springer, New York, First edition, 2003.
- [26] K.N. Premnath and J. Abraham. Three-dimensional multi-relaxation time (mrt) lattice-boltzmann models for multiphase flow. *Journal of Computational Physics*, 224(2):539–559, 2007.
- [27] A. Prosperetti and G. Tryggvason. *Computational Methods for Multiphase Flow*. Cambridge University Press, New York, First edition, 2007.
- [28] M. Rudman. Volume-tracking methods for interfacial flow calculations. *International Journal for Numerical Methods in Fluids*, 24(7):671–691, 1997.
- [29] Xiaowen Shan. Pressure tensor calculation in a class of nonideal gas lattice boltzmann models. *Phys. Rev. E*, 77:066702.
- [30] Xiaowen Shan. Analysis and reduction of the spurious current in a class of multiphase lattice boltzmann models. *Phys. Rev. E*, 73:047701, Apr 2006.
- [31] Xiaowen Shan and Hudong Chen. Lattice boltzmann model for simulating flows with multiple phases and components. *Phys. Rev. E*, 47:1815–1819, 1993.
- [32] Y. Shi, T.S. Zhao, and Z.L. Guo. Lattice boltzmann method for incompressible flows with large pressure gradients. *Physical Review E - Statistical, Nonlinear, and Soft Matter Physics*, 73(2), 2006.
- [33] M. Sussman. A level set approach for computing solutions to incompressible two-phase flow. *Journal of Computational Physics*, 114(1):146–159, 1994.
- [34] M. Sussman, E. Fatemi, P. Smereka, and S. Osher. An improved level set method for incompressible two-phase flows. *Computers and Fluids*, 27(5-6):663–680, 1998.
- [35] G. Thommes, J. Becker, M. Junk, A.K. Vaikuntam, D. Kehrwald, A. Klar, K. Steiner, and A. Wiegmann. Numerical investigation of a combined lattice boltzmann-level set method for three-dimensional multiphase flow. *International Journal of Computational Fluid Dynamics*, 23(10):687–697, 2009.
- [36] D. Yu, R. Mei, L.-S. Luo, and W. Shyy. Viscous flow computations with the method of lattice boltzmann equation. *Progress in Aerospace Sciences*, 39(5):329–367, 2003.
- [37] Zhao Yu and Liang-Shih Fan. Multirelaxation-time interaction-potential-based lattice boltzmann model for two-phase flow. *Phys. Rev. E*, 82:046708, 2010.
- [38] P. Yuan and L. Schaefer. Equations of state in a lattice boltzmann model. *Physics of Fluids*, 18(4), 2006.